EXPERIMENTAL INVESTIGATION OF BUBBLE GROWTH ON A SINGLE ARTIFICIAL NUCLEATION SITE IN MICROGRAVITY CONDITIONS: INFLUENCE OF THE LIQUID SUBCOOLING AND NON-CONDENSABLE RESIDUALS

Lounès Tadrist

Proceedings of the 17th International Heat Transfer Conference, IHTC-17
14 – 18 August 2023, Cape Town, South Africa

IHTC-17 | ID: 0896

EXPERIMENTAL INVESTIGATION OF BUBBLE GROWTH ON A SINGLE ARTIFICIAL NUCLEATION SITE IN MICROGRAVITY CONDITIONS: INFLUENCE OF THE LIQUID SUBCOOLING AND NON-CONDENSABLE RESIDUALS

Fedor Ronshin[1*], Oleg Kabov[1], Alexey Rednikov[2], Lounes Tadrist[3]

[1]Kutateladze Institute of Thermophysics, Av. Lavrentyev, 1, Novosibirsk 630090, Russia
[2]Université libre de Bruxelles, TIPs, CP 165/67, Av. F.D. Roosevelt 50, 1050 Brussels, Belgium
[3]Aix Marseille Université, CNRS, Laboratoire IUSTI, UMR 7343, 13453 Marseille, France

ABSTRACT

The purpose of this work is to study the boiling heat transfer mechanisms in microgravity. Subcooling is one of the important parameters defining the bubble growth process. In this work, we have analyzed the effect of subcooling on bubble nucleation and growth. The bubble diameter was evaluated in time using the developed algorithm. Several stages of bubble growth were highlighted. The effect of subcooling on the bubble growth rate was analyzed. It is shown that subcooling has a significant effect on all stages of bubble growth. A numerical model has been developed to help the better understanding of the bubble growth phenomena. The numerical and experimental results have been compared to analyze the effect of subcooling on bubble growth. Some observations couldn't be explained without evoking the presence of non-condensable residuals. The amount of these was estimated.

KEY WORDS: Single bubble growth, boiling, microgravity, subcooling, bubble collapse, non-condensable

1. INTRODUCTION

Boiling still remains one of the hot topics in science nowadays. Although the process of boiling is widely encountered both in everyday life and in many practical applications (energy conversion, chemical industry, space industry, and others), this process is complex and poorly understood. Pioneering work in this field goes back to Nukiyama's study in 1934 [1]. He was the first to propose the boiling curve. This curve characterizes the heat transmitted from the wall to the boiling liquid and provides a relationship between the heat transfer and the boiling regimes. The majority of the studies are experimental having an empirical character because of the complexity of the mechanisms involved (heat transfer coupling, nucleation, bubble dynamics, natural convection, evaporation, condensation, contact line dynamics, wettability, thermocapillary and nonequilibrium effects). In most cases, the authors provide characteristics curves of the heat transfer and correlations for applications such as the design of evaporators, steam generators, thermosiphons, and heat pumps. Among these studies, several authors have proposed correlations for evaluating the heat flux density based on the thermo-physical properties of the fluid and the wall [2-7]. Detailed investigations of the single vapor bubble growth dynamics as a function of the experimental conditions are limited [8-15].

The purpose of this work is to study the boiling heat transfer mechanisms. This problem is multi-dimensional, with several interacting parameters. Among them, gravity is one of the most important parameters since the densities of the liquid and vapor phases differ by almost three orders of magnitude. To get rid of an overwhelming influence of this parameter, a microgravity boiling research program was

*Corresponding Author: f.ronshin@gmail.com

implemented and supported by the European Space Agency [16]. For several years, an international science team has been working on this program. The RUBI experiment (Reference mUltiscale Boiling Investigation) was created and tested on Earth at the end of 2018 and delivered to the International Space Station in July 2019.

The RUBI experiment was created for investigation of the boiling process in its most elementary form, namely, in the form of a single vapor bubble in a pure liquid with well-controlled conditions. The objectives of the RUBI experiment are to study: - heat transfer in the region of the contact line of a single vapor bubble; -dynamics of bubble growth; -boiling with shear flow [17,18]; -boiling in the presence of an electric field [16]. The experiment focuses on the relationship between the macroscopic dynamics of bubbles (nucleation, growth, detachment) and microscopic phenomena at the contact line.

This paper presents the investigation of the bubble behavior in pool boiling conditions of the RUBI experiment in microgravity ($< 10^{-4} g$). The liquid motion is induced by the bubble growth-collapse. The experiments carried out on board the International Space Station allow us to observe the movements of the bubbles generated by liquid-vapor phase change. The behavior of bubbles is studied mainly by image analysis of the movies obtained by the camera. These images allow for each experiment to determine the characteristics of bubbles according to the operating conditions. In support of these experimental works, a simplified numerical model allows us to predict the behavior of the bubbles in the operating conditions of the experiment. First original conclusions on the behavior of vapor bubbles in microgravity conditions are proposed. A conjecture of the presence of non-condensable residuals is put forward as a result of the analysis.

2. EXPERIMENTAL SETUP AND PROCEDURE

A detailed description of the experimental setup and methods is presented in [16]. In this section, we present the main components of this device and the associated measurement techniques used. The core of the RUBI experiment is the boiling cell with an integrated forced convection loop (FCL). A thin foil heater (chromium layer of thickness ~200 nm) is coated on top of a BaF_2 plate (thickness 5 mm) playing the role of the substrate. The boiling process takes place at the foil heater, initiated by locally superheating an artificial nucleation site (depth ~100 μm inside the BaF_2 substrate) using a focused laser spot (BaF_2 being transparent). The temperature distribution of the heating foil is measured from the back side by IR thermography while the bubble shapes are observed via a side high-speed camera. The temperature inside the bubble and in the vicinity of the liquid-vapor interface is supposed to be measured by a rack of four micro-thermocouples.

The boiling cell (Figure 1) is equipped with a thermal control system allowing a homogeneous thermalization of the working fluid N-perfluorohexane (the primary component of FC-72) in the range from 30°C to 70°C. Two stimuli systems may be used to apply forces on the vapor bubbles: an electric field induced by a washer-shaped electrode positioned (distance from the heater from 6 to 10 mm) above the substrate, adjustable in strength (0 to 15 kV), and a shear flow (0 to 0.5 L/min) that is created by the FCL.

A technique for the automatic analysis of experimental images has been developed. A detailed description of the technique is presented in reference [19]. The algorithm analyses the shape of the bubble, calculates its diameter, contact line diameter, and contact angle. The analysis includes the following stages: binarization (analysis of brightness and contrast), finding the baseline, determining the bubble contour, and determining the parameters of the bubble using various approximations. In the absence of external forces (shear flow and electric field), the bubble has a spherical shape. Figure 2 shows the typical images during bubble analysis.

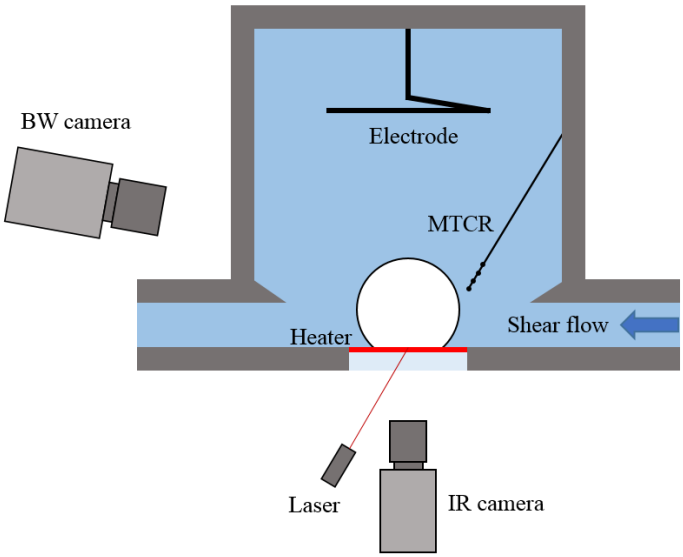

Fig. 1 Scheme of the RUBI boiling cell.

After the main steps of background subtraction and image binarization, this algorithm uses Matlab functions to improve the image. For this, the algorithm first converts all black pixels that are enclosed within the white pixels of the bubble contour into white ones (see 2nd and 3rd segments of Figure 2). The function *strel* creates the structural element (disk with diameter 1-2 pixels), that is used in the *imopen* function to reduce the noise of the bubble surface. The *regionprops* function is used to detect all bubbles in the frame. Further, there is a separate processing for each bubble. The parameters of the bubble are compared with the bubbles from the previous frame, and the correspondence with the bubble at the previous is determined. If, when comparing the parameters of the bubble, the corresponding bubble in the previous frame is not determined, then the bubble is considered newly formed. It is considered that a bubble can only form at the nucleation point. After that, each bubble is investigated. The baseline is determined for each bubble using its reflection. The baseline is the line of the bubble foot location on the surface. Since bubbles can move along the plane of the heater, their baselines may differ. Before the final determination of bubble edges, the present algorithm extracts the pixels of bubble reflection from the images. The part of the binary image that is located below the detected bubble foot is cropped, and the bubble contour is determined, using the Matlab functions (Figure 3, 4th segment).

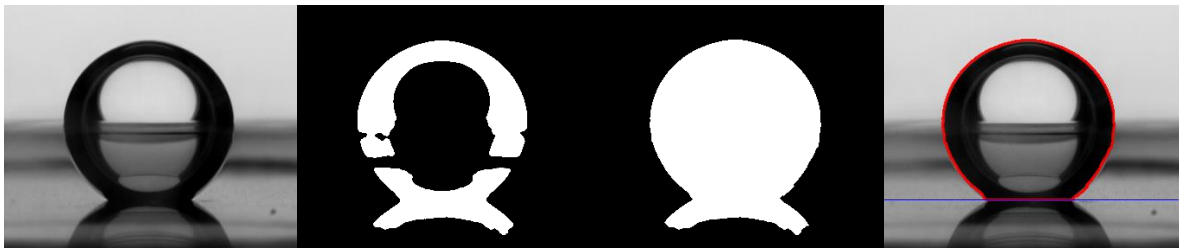

Fig. 2 The steps of algorithm for the detection of bubble contour at the BW RUBI images: (a) original image; (b) binarized image; (c) improved binarized image; (d) detected bubble contour.

This algorithm defines bubble diameter as the maximum horizontal distance between the bubble contour side points. The contact line diameter is still considered as the horizontal distance between the left and the right contact points.

3. MODEL

To rationalize the experimental findings, a simple axisymmetric model has been developed as schematized in Fig. 3. It assumes a sessile bubble in the form of a spherical cap, which is indeed a good approximation for the pool boiling runs beyond some initial shape oscillations [20]. The contact angle θ is assumed to be a priori given and fixed. Its value in the computations is set to a reasonable mean value adopted from the experiment (here 24°), whereas it has been shown that the result for the bubble diameter as a function of time is only marginally sensitive to this value.

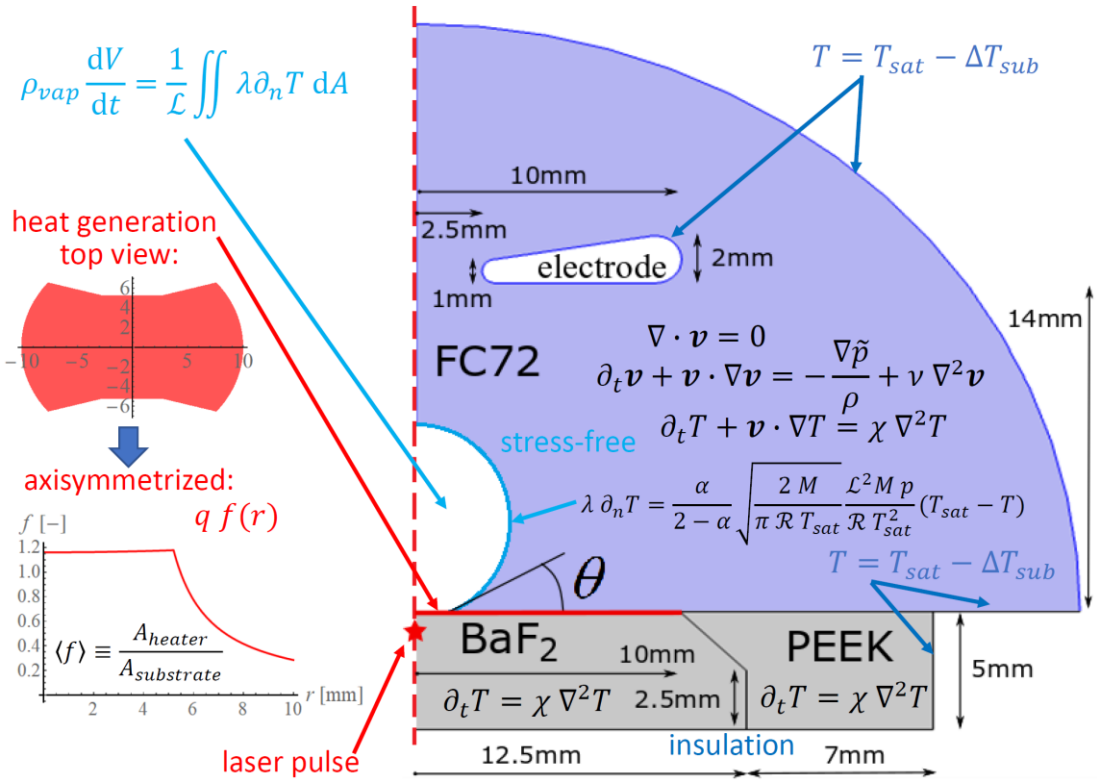

Fig. 3 Schematic of the model. Equations and boundary conditions are mentioned on this figure.

The interior of the bubble is assumed dynamically passive and heat transfer through it is disregarded. The heat transfer governing the bubble growth, or more generally the bubble size evolution, is then realized through the liquid, where a full set of Navier-Stokes and convective heat transfer equations is solved. A separate equation for the bubble size evolution is set, according to which the mass of the vapor (at a specified ambient pressure P, here 600 mbar, and the corresponding saturation temperature T_{sat}, here 42.4°C) varies in time in accordance with the integral heat flux from the liquid divided by the latent heat. At the bubble surface, a Schrage-type kinetic equation is used with the accommodation coefficient α equal to unity. This results in the bubble surface temperature practically equal to T_{sat} except for a tiny vicinity of the contact line (of the order of tens of nm), where the kinetic effect of evaporation is significant due to large local flux densities. Other than that, no nano/microscopic effects at the contact line are incorporated (no 'microregion'). Heat transfer in the solid substrate, involving a BaF_2 plate and an adjacent PEEK layer is considered in full in accordance with RUBI specifications. The only exception is that the heat generation distribution atop the BaF_2 plate, in a sub-microscopic coated heater treated of a zero thickness here, is additionally axisymmetrized towards the BaF_2 substrate edge by taking the mean value at each concentric circle (the RUBI heater coating, shown by its top view in Fig. 3, is not axisymmetric even if the BaF_2 substrate itself is). Furthermore, the heat generation density therein is not fully uniform (due to a non-uniform electric current in this geometry), the computation data for which is adopted from [21] and which is also accounted for in the axisymmetrization procedure. The mean and

integral values of the generated heat are thereby maintained as specified in RUBI. The nucleation process as such is not modelled. Rather, a small initial bubble (~60μm in diameter) is inserted at the moment right after t_{wait}, in the beginning of the laser pulse. The laser pulse is modelled by a nearly point heat generation uniformly distributed within a sphere of 30 μm and acting during the pulse time of 10 ms or 20ms at a depth of 100μm (the nucleation site depth according to RUBI specifications) in BaF_2. The simulations are carried out with the help of COMSOL Multiphysics software.

4. RESULTS AND DISCUSSION

In this work, we investigated the bubble growth dynamics at the pressure P = 600 mbar (which corresponds to T_{sat}=42.4°C) and heat flux q = 0.5 W/cm^2. Liquid subcooling (below T_{sat}) was varied from $\underline{\Delta}T_{sub}$ = 1°C to 5°C. The heater was activated t_{wait} =1 s before bubble initiation by the laser. Laser pulse time was equal to 10 ms for $\underline{\Delta}T_{sub}$ = 1°C and 20 ms for $\underline{\Delta}T_{sub}$ = 3°C and 5°C. The bubble behavior was visualized during 9 s after the laser pulse.

4.1 Bubble formation.

Figure 4 shows the images of the bubble formation process for different subcooling. At the bottom of each image, the time from the start of the laser pulse is shown. The laser causes local overheating at the nucleation point. The upper row shows the bubble patterns for the smallest subcooling (close to the saturation condition). The bubble forms at 0.008 s (with an uncertainty of 0.002 s attributable to the acquisition rate of 500 fps) after laser initiation. The laser pulse duration is 10 ms, which corresponds to the image at 0.010 s. The bubble is deformed during its rapid growth after nucleation. In the first image immediately after formation, the bubble has an oblate shape, elongated along the horizontal axis. Then, under the influence of surface tension forces, the bubble tends to acquire a spherical shape. Oscillations occur under the action of inertia forces and surface tension (the time scale $\sqrt{\rho\, D^3/\gamma}$ capturing well the order of magnitude of the period) and the bubble assumes a prolate shape, elongated along the vertical axis. The oscillation amplitude being sufficiently large, this can lead to the bubble bouncing off the surface. When the bubble detaches, vapor remains in the cavity. A new bubble immediately forms as a result. The detached bubble is located at some distance from the surface. When the newly formed bubble reaches a sufficient size to touch the detached bubble, coalescence occurs. Herewith, the larger, detached bubble moves closer to the surface (perhaps, partly due to the center-of-mass shift after the coalescence, partly due to its further growth). The cycle is then repeated until it reattaches to the substrate. After that, there is a monotonous growth of the bubble. The last image in a row shows the time when the bubble stabilizes (the bubble is attached and the contact angle is stabilized).

The middle and bottom rows in figure 3 illustrate the effect of subcooling on the initial stage of bubble life. It is seen that the nucleation time significantly increases with the increase in subcooling since the laser needs to transfer more energy to the fluid. At the intermediate subcooling, the bubble stays attached to the substrate. Yet, at the high subcooling, a detached bubble is observed once again, which might be due to a sufficient decrease in the bubble-growth factor favoring the attachment. For this high subcooling, bubble reduction in size (i.e. vapor condensation) is observed after the laser pulse stopped (at 20 ms), which indicates that as the laser heat has dissipated the substrate is not yet sufficiently heated up. However, the attached bubble does not vanish completely, nor the detached (upper) bubble located at a height h_{upper}~1.5 mm above the substrate. This upper bubble rapidly decreases in size at first, but then stays practically unchanged for quite a long time (several seconds). Our conjecture is that such a long survival owes itself to the presence of some residuals of non-condensable gases (in spite of careful degassing of the working liquid), cf. an estimation in the following paragraph. The penultimate image in the third row shows the minimum size of the attached bubble. After a while, the attached bubble grows under the heating. In contrast, as already mentioned, the upper bubble keeps its state much longer, until t~3.5 s (not shown in the figure), when it starts a downward motion, barely noticeable at first, and then progressively accelerates and rapidly (within ~0.5 s) merges the (by then) well larger attached bubble. We speculate that it is by that time that the developing thermal boundary layer from the heater reaches its position, which view is quite

consistent with a thermal-diffusion time scale $h_{upper}^2/4\chi \sim 18\,s$. The downward motion may then be caused by the thermal Marangoni (thermocapillary) drift in the direction of an external temperature gradient, which mechanism for bubbles was first pointed out in [22]. The presence of non-condensables is herewith quite essential (otherwise the Marangoni effect would have been inhibited by a practically constant temperature at the bubble surface). Conversely, the fact of observing such a drift can be interpreted as yet another evidence in favor of their presence.

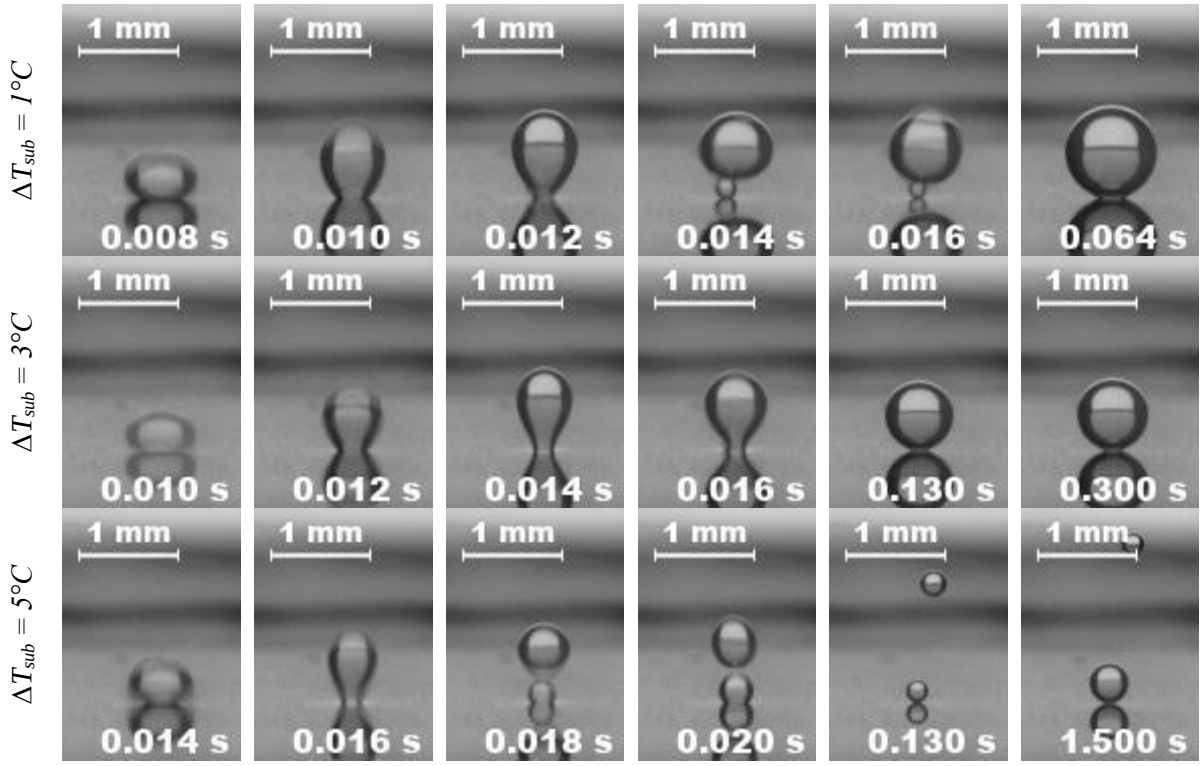

Fig. 4 The effect of subcooling ΔT_{sub} on bubble nucleation and stabilization. P = 600 mbar, q = 0.5 W/cm^2, t_{wait} =1 s, laser pulse 10 ms (top row) and 20 ms (middle and bottom rows). The time indicated at each image is counted from the laser pulse start. The first image in each row shows the first bubble observed after nucleation.

The upper bubble in the third row of Fig.4 can be used for an estimation of the amount of non-condensable gases, which we conjectured to be present in the system. Let V_{ini} be the 'initial' volume of the upper bubble upon its detachment, while V_{fin} roughly its 'final' volume upon its stabilization after the earlier mentioned rapid initial decrease in size. The partial vapor pressure in this final state is estimated as $P_{sat}(T_{sat} - \Delta T_{sub})$, where $P_{sat}(T)$ is the saturation curve, such that $P_{sat}(T_{sat}) \equiv P$. Then the final partial pressure of non-condensables is $P - P_{sat}(T_{sat} - \Delta T_{sub})$, whereas the initial one will roughly be $\big(P - P_{sat}(T_{sat} - \Delta T_{sub})\big)V_{fin}/V_{ini}$ (neglecting, in particular, the back dissolution during the observation time). Using $T_{sat} = 42.4°\mathrm{C}$, $\Delta T_{sub} = 5°\mathrm{C}$ and FC-72 saturation data yields $P_{sat}(T_{sat} - \Delta T_{sub}) = 494\ \mathrm{mbar}$. By image processing, we obtain $V_{ini}/V_{fin} \sim 10$. Then, with $P = 600\ \mathrm{mbar}$, the partial pressure of non-condensables in the initial state is estimated at a level of 10 mbar (out of 600 mbar), and hence the non-condensable molar fraction inside a growing bubble is estimated at ~2%. This is not large and confirms a high quality of degassing (especially given that nitrogen is highly soluble in FC-72, at ~50% volume fraction at normal conditions). Yet this may be crucial to ensure the bubble survival and other effects discussed above. We shall come back to this point later on.

4.2 Three stages.

Figure 5 shows the bubble diameter evolution in time in linear and logarithmic scales for the smallest subcooling value. In linear scale, the zero-time moment corresponds to the laser pulse beginning. The initial bubble diameter after nucleation is about 0.7 mm. After nucleation, rapid bubble growth is observed. Then the vapor bubble growth law changes. To analyze bubble growth dynamics, the bubble diameter is plotted in a logarithmic scale. In Fig. 5b, the zero time corresponds to bubble nucleation. The bubble diameter was approximated by a power dependence by the least squares method. The bubble growth can be separated into several stages. The first, from 0 to 62 ms, is a zone in which rapid bubble growth is observed under the influence of the laser pulse. At this stage, the bubble grows in superheated liquid and the bubble form is not spherical. The time exponent for this case is 0.23. The second stage is a transition one, when the bubble acquires a spherical shape and continues to grow, it lasts until t=1.5s and the exponent is 0.63. The boundary of this stage is determined by the change in the vapor bubble growth law. And the third stage, when the exponent differs from the second stage. For this case, it is equal to 0.77. The third stage lasts for a quite long time (up to the end of the experiment), during which there is a uniform growth of the bubble. This stage corresponds to the bubble growth largely outside the thermal boundary layer from the heater.

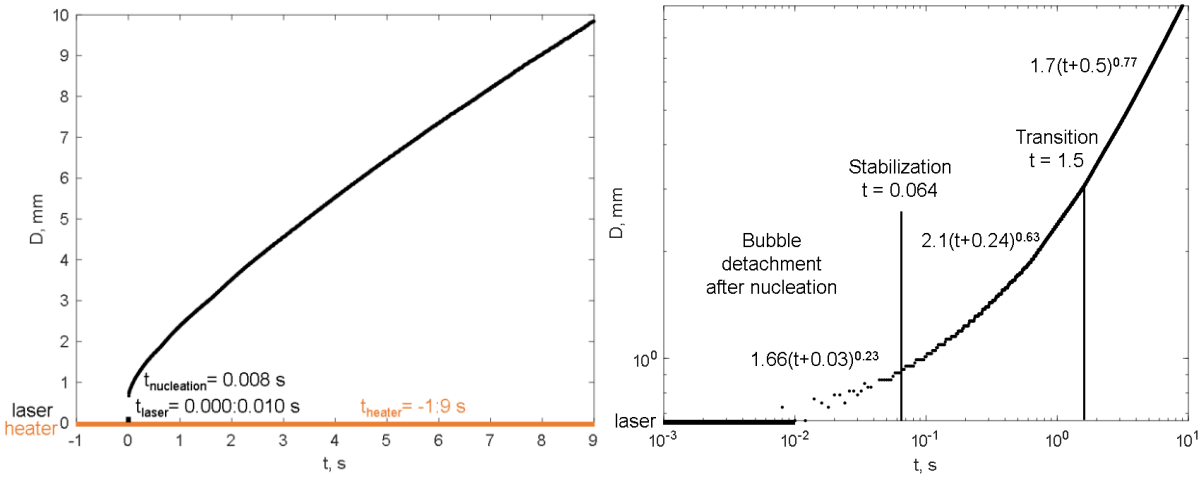

Fig. 5 Horizontal bubble diameter evolution in time for P = 600 mbar, q = 0.5 W/cm^2, *and* ΔT_{sub} = 1°C **a)** linear scale and **b)** logarithmic scale. Color text "laser" and "heater" and color bars show the period when the laser and heater are activated. Power laws show the typical bubble growth ones for different stages.

The influence of subcooling on bubble growth dynamics is shown in figure 6. During the first stage, the bubble increases due to the influence of the laser pulse. For high subcooling ($\Delta T_{sub} = 5°C$), the bubble begins to condense immediately after the nucleation. For moderate subcooling ($\Delta T_{sub} = 3°C$), the bubble begins to condense after the laser pulse. The bubble condensation is also observed during the second stage for $\Delta T_{sub} = 3°C$ and $5°C$. For a thin superheated liquid layer, evaporation is deemed to occur just in the contact line region. Then the liquid superheated layer sufficiently increases, and the bubble growth is observed. In the third stage of the bubble growth, the time exponent increases closer to 1 with the increase of the subcooling.

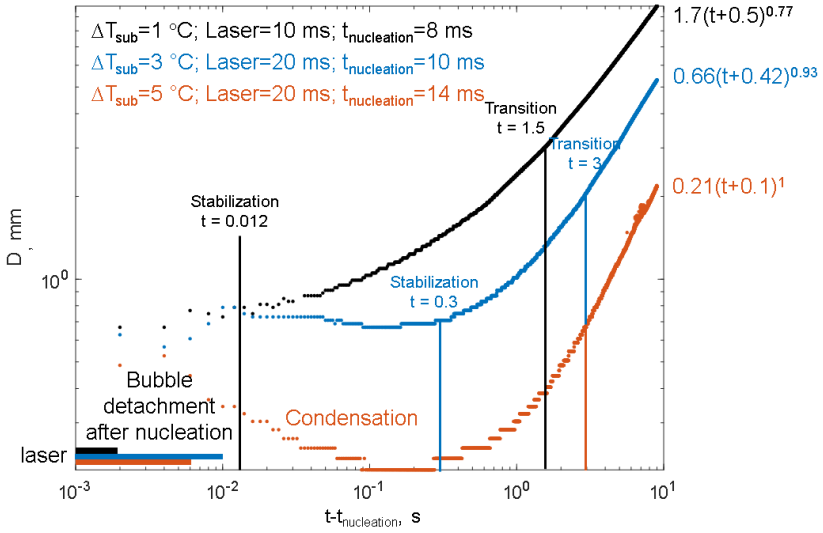

Fig. 6 Horizontal diameter of the attached bubble versus time. The effect of subcooling on the bubble growth for several subcooling temperatures. The text "laser" and color bars show the period when the laser is activated. Power laws represent the typical bubble growth for the third stage.

4.3 Comparison with simulations.

To analyze the bubble growth behavior, we have compared the experimental results with the simulation. Figure 7 shows the subcooling effect on the bubble growth calculated by the model of section 3.

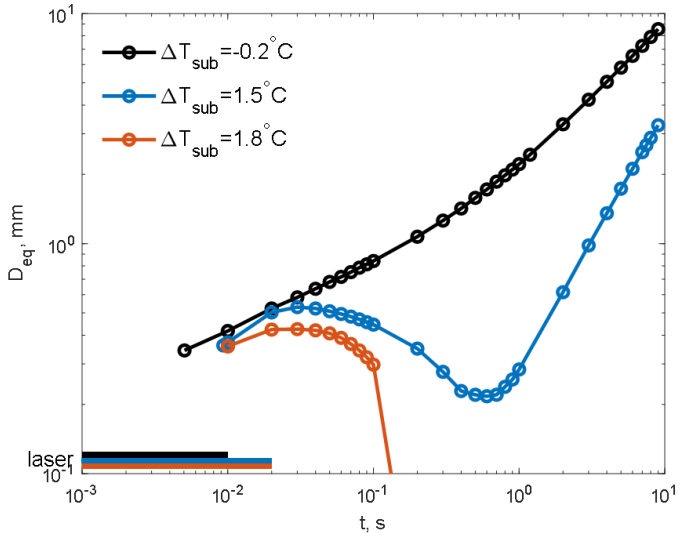

Fig. 7 Calculated equivalent diameter of the bubble versus time. The effect of subcooling on the bubble growth. Simulation results. P = 600 mbar, q = 0.5 W/cm^2, t_{wait} =1 s, laser pulse 10 ms (top curve) and 20 ms (middle and bottom curves).

The case at a nearly saturation condition (overheating at ΔT_{sub} = -0.2°C) turns out to be very close to the experimental result for ΔT_{sub} = 1°C. Yet we see that a lower subcooling (by roughly 1.2°C) was required in the simulations to reproduce well the experimental result. Such an effective subcooling shift in simulations relative to the experiment is quite in agreement with what was also found by other RUBI partners at other parameter sets [23]. As far as higher subcoolings are concerned, the simulation with ΔT_{sub} = 1.5°C was able to reproduce a situation with a temporary bubble crisis (vapor condensation) before its growth resumes. However, once again, this happens in the simulations at a lower subcooling than in the experiment. Furthermore, in the simulations, the bubble is seen to totally collapse already at ΔT_{sub} = 1.8°C, whereas in

the experiment it survives even at ΔT_{sub} = 5°C. Here we come back to the conjecture made in subsection 4.1 concerning a possible presence of small amounts of non-condensable gases helping the bubbles to survive, and state that the results of the simulations (with no non-condensables in the model) point in favor of such a conjecture. Another evidence to the same effect is provided by a simulation without a bubble, where it has been found that for ΔT_{sub} = 5°C the substrate temperature by the end of the experiment (i.e. at $t = 9$ s) does not even reach T_{sat} (incidentally, by ~1.2°C). Therefore, the eventual bubble growth observed in the experiment for ΔT_{sub} = 5°C would not be possible to explain unless a hypothesis like the mentioned one was evoked. Other factors may have also contributed to the disagreement. For instance, given the sensitivity to the subcooling value, any possible imprecision in the saturation data may be quite perceptible [24]. Moreover, the accuracy of determining subcooling in the experiment is 0.5°C, which can also cause such differences.

5. CONCLUSIONS

In this paper, we present the results on the bubble growth for different liquid subcooling values in microgravity. Three stages were highlighted during the bubble growth. The effect of subcooling on bubble nucleation and growth was analyzed in the range of ΔT_{sub} = 1°C - 5°C. It is shown that with an increase in subcooling, the bubble becomes more prone to condensing after the nucleation. Later the bubble begins to grow rapidly. For the third stage, the exponent of bubble growth becomes closer to one for higher subcooling values. This is also confirmed by numerical calculations. As a result, subcooling has a significant impact on all stages of bubble growth. Comparison with the calculation showed that there may be a small amount of non-condensable gases in the liquid, which also influences the growth and survival of the bubble.

ACKNOWLEDGMENT

The present work has been carried out in the framework of the European Space Agency Research projects AO-2004-111: BOILING, AO-1999-110: EVAPORATION, AO-2004-096: CONDENSATION. For space reasons, the complete acknowledgement is reported in http://www.den.unipi.it/paolo.dimarco/eps/RUBI-ack.pdf
Co-authors from Kutateladze Institute of Thermophysics would like to acknowledge funding by the Russian Science Foundation (Project No. 21-79-10357).
AR thanks Julie Jambert from Toulouse INP-ENSEEIHT for a substantial contribution to the numerical code development during her internship at ULB-TIPs, as well as acknowledges the funding from BELSPO PRODEX Heat Transfer.
Co-authors from Aix-Marseille Université – IUSTI gratefully acknowledge the CNES (Centre National d'Études Spatiales) for the financial support of the present study.
Co-authors from Aix-Marseille Université – IUSTI gratefully acknowledge the ANR (Agence National de la Recherche) for the financial support of the present study.

NOMENCLATURE

D	bubble diameter	[mm]
$D_{eq}=(6V/\pi)^{1/3}$	bubble equivalent diameter	[mm]
t	time	[s]
t_{wait}	waiting time	[s]
T_{sat}	saturation temperature	[°C or K]
T_{liquid}	liquid temperature	[°C or K]
$\Delta T_{sub}=T_{sat}-T_{liquid}$	subcooling degree	[°C]
V	bubble volume	[mm^3]

REFERENCES

[1] Nukiyama, S., "The maximum and minimum values of the heat transmitted from metal to boiling water under atmospheric pressure," *Int. J. Heat Mass Transf.*, 27(7), pp. 959-970, (1934).

[2] Kutateladze, S. S., "Boiling heat transfer," *Int. J. Heat Mass Transf.*, 4, pp. 31-45, (1961).

[3] Rohsenow, W. M., "A method of correlating heat-transfer data for surface boiling of liquids," *Transactions of the American Society of Mechanical Engineers*, 74(6), pp. 969-975, (1952).

[4] Han, C. Y., and Griffith, P. "The mechanism of heat transfer in nucleate pool boiling—Part I: Bubble initiaton, growth and departure," *Int. J. Heat Mass Transf.*, 8(6), pp. 887–904, (1965).

[5] Cooper, M. G., "The microlayer and bubble growth in nucleate pool boiling," *Int. J. Heat Mass Transf.*, 12(8), pp. 915–933, (1969).

[6] Stephan, P., *B1 Fundamentals of Heat Transfer*, Springer Berlin Heidelberg, Berlin, Heidelberg, pp 15–30, (2010).

[7] Gorenflo, D., *Pool Boiling*, VDI Heat Atlas, Chap. Ha, VDI Verlag, Dusseldorf, Ha1–Ha25, (1993).

[8] Siegel, R., and Keshock, E. G., "Effects of reduced gravity on nucleate boiling bubble dynamics in saturated water," *AIChE Journal*, 10, pp. 509-517, (1964).

[9] Qiu, D. M., Dhir, V. K., Chao, D., Hasan, M. M., Neumann, E., Yee, G., and Birchenough. A., "Single-bubble dynamics during pool boiling under low gravity conditions," *Journal of Thermophysics and Heat Transfer*, 16, pp. 336-345, (2002).

[10] Duhar, G., and Colin, C., "Dynamics of bubble growth and detachment in a viscous shear flow," *Physics of Fluids*, 18(7), p. 077101, (2006).

[11] Kim, J., and Kim, M. H., "On the departure behaviors of bubble at nucleate pool boiling," *International Journal of Multiphase Flow*, 32(10-11), pp. 1269-1286, (2006).

[12] Kim, J., "Review of nucleate pool boiling bubble heat transfer mechanisms," *International Journal of Multiphase Flow*, 35(12), pp. 1067-1076, (2009).

[13] Colin, C., Kannengieser, O., Bergez, W., Lebon, M., Sebilleau, J., Sagan, M., and Tanguy, S., "Nucleate pool boiling in microgravity: recent progress and future prospects," *Comptes Rendus Mécanique*, 345(1), pp. 21-34, (2017).

[14] Surtaev, A., Serdyukov, V., Zhou, J., Pavlenko, A., and Tumanov, V. "An experimental study of vapor bubbles dynamics at water and ethanol pool boiling at low and high heat fluxes," *Int. J. Heat Mass Transf.*, 126, pp. 297-311, (2018).

[15] Surtaev, A., Serdyukov, V., and Malakhov, I., "Effect of subatmospheric pressures on heat transfer, vapor bubbles and dry spots evolution during water boiling," *Experimental Thermal and Fluid Science*, 112, p. 109974, (2020).

[16] Sielaff, A., Mangini, D., Kabov, O., Raza, M. Q., Garivalis, A. I., Zupančič, M., ... and Tadrist, L., "The multiscale boiling investigation on-board the International Space Station: An overview," *Applied Thermal Engineering*, 205, p. 117932, (2022).

[17] Bucci, M., Zupančič, M., Garivalis, A. I., Sielaff, A., Di Marco, P., and Golobič, I., "The role of the electric field in the departure of vapor bubbles in microgravity," *Physics of Fluids*, 35(1), p. 017109, (2023).

[18] Garivalis, A. I., and Di Marco, P., "Isolated bubbles growing and detaching within an electric field in microgravity," *Applied Thermal Engineering*, 212, p. 118538, (2022).

[19] Oikonomidou, O., Evgenidis, S., Argyropoulos, C., Zabulis, X., Karamaounas, P., Raza, M. Q., ... and Karapantsios, T., "Bubble growth analysis during subcooled boiling experiments on-board the International Space Station: Benchmark image analysis," *Advances in Colloid and Interface Science*, 308, p. 102751, (2022).

[20] Ronshin et al., Investigation of bubble growth on a single artificial nucleation site near saturation conditions in microgravity, to be published.

[21] Schinnerl, M. et al. "Heat transfer in single bubble nucleate boiling within the multiscale boiling project onboard the International Space Station". In: *Proceedings of the 17th International Heat Transfer Conference*, 14—18 August 2023, Cape Town, South Africa.

[22] Young, N. O., Goldstein, J. S., and Block, M. J., "The motion of bubbles in a vertical temperature gradient," *J. Fluid Mech.*, 6, pp. 350-356, (1959).

[23] Torres, L., and Colin, C., Private communication, (2023).

[24] Kind, J., and Sielaff, A., Private communication, (2023).